Hindawi Publishing Corporation
Journal of Sensors
Volume 2012, Article ID 693082, 9 pages
doi:10.1155/2012/693082

*Research Article*

# Development of a Nondestructive Impulse Device and Damage Model for Unreinforced Concrete

**Shane D. Boone, Paul J. Barr, James A. Bay, and Marvin W. Halling**

*Department of Civil and Environmental Engineering, Utah State University, 4110 Old Main Hill, Logan, UT 84332-4110, USA*

Correspondence should be addressed to Paul J. Barr, paul.barr@usu.edu

Received 4 November 2011; Accepted 15 January 2012

Academic Editor: Shenfang Yuan



Unconstrained compression waves were measured using a newly developed, nondestructive, short impulse excitation device developed for long-term structural health monitoring. The measurements, using this innovative device, were used to determine the variation in the first longitudinal modal frequency as a function of loading magnitude and loading cycles to failure of various concrete mixes. Longitudinal frequency and cumulative energy variations were found to be a function of concrete compressive strength. These results imply that higher-strength concrete more easily absorbs energy and restricts the growth of microcracks. Based on the results, a new damage model is proposed that was shown to correlate with measured values to within 7%. This proposed model was found to have a closer correlation than Miner's hypothesis and damage index models from other reviewed research.

## 1. Introduction

Testing methods that determine the in-place physical properties of concrete structures are important tools for engineers to quantify their capacity and long-term performance. Code-based procedures that result in the evaluation of the integrity of existing structures depend on accurate material properties to correctly determine the condition of these structures. Currently, there are many such methods (i.e., stress wave propagation methods) in existence that allow engineers to determine these material properties. However, these tools and techniques have been developed based on the assumption that dynamic material measurements are not affected by the inherent stress history applied to structures due to self-weight, super-imposed dead loads, and live loads. Such loading causes fatigue and damage in the form of microcracking that can change the long-term structural health with regard to wave propagation. These long-term changes in the propagation velocities of stress waves must be clearly understood so that nondestructive measurements of existing structures are not only quantitative but also correctly analyzed.

In the case of a heterogeneous material like concrete, the assumption that it is homogenous is accepted in order for the basic theories and techniques of stress wave propagation methods to be applicable. However, the measured stress waves are typically too large in length to determine properties such as porosity, interfacial bond quality between aggregate and matrix material, or the presence of microcracks. Instead, the wave characteristics measured during these tests represent the average physical properties of the concrete structure or specimen analyzed (i.e., a homogenous measurement).

When concrete is loaded with any significant amount of stress, tensile stresses are produced and microcracks form. Stress, in this case, can result from any type of loading, including those induced during the curing process such as bleeding, settling of grout, and shrinkage. These stress-induced cracks typically initiate around the aggregate-to-matrix interfaces and then progress as additional loads are applied. It is this microcrack growth and coalescence that causes the failure of concrete [1]. Because the accumulation of microcracks leads to the failure of concrete, it is reasonable to assume that the accumulation of these cracks is a good indicator of damage.

Several methods have been developed to predict the damage in concrete structures due to loading. The majority of these models use energy-related damage indicators to

quantitatively assess the damage in such structures [2–5]. Also, other researchers [6] have developed relationships for the calculation of fatigue of unreinforced concrete to incorporate indicators such as stress versus number of cycles, ratio of minimum to maximum stress, and rate of loading. Other predictive models have used various indicators such as splitting tensile strength [7], stress-strain relationships [8–10], and strain-cycle relationships [11].

As cycling and fatigue loading is applied to concrete, the primary reason for a decrease in the structural-related properties is the continuous microcrack growth. Thus, research interest to investigate procedures to measure the growth of these cracks has been conducted [12–14]. All of these studies have incorporated nondestructive testing (NDT) techniques to quantify crack growth as a function of loading cycles. Measurements of pulse velocity, acoustic emission, and ultrasonic wave attenuation are methods that have been used to determine the growth of microcracks. All of these methods use similar techniques that initially excite the specimens and subsequently measure the elastic wave characteristics of the material during and after the specified loading cycles. The free-free resonant column (FFRC) method has traditionally been used to quantify damage in terms of the fundamental longitudinal, transverse, and torsional frequencies as well as damping [15]. The results from all of the NDT research indicate that measurements of elastic wave properties are a good indicator of damage in concrete.

A more recent study [16] indicates that the elastic properties of the material are dependent not only on the growth of microcracks but also on the closing of microcracks. Some researcheres [16] have shown in a feasibility study that surface wave velocities propagating parallel to the direction of loading demonstrate a distinct stress sensitive behavior. During this study, surface wave velocities were measured while concrete specimens were uniaxially loaded to 35% and 80% of the ultimate compressive strength. Results indicate that as stress levels increase, microcracks in the specimens close and the surface wave velocities increase.

There is also an anisotropic behavior of elastic waves in loaded concrete specimens that depends on the direction of loading relative to the direction of wave propagation [16]. Thus, the presence of microcracks forming in the same direction of loading can be measured by determining the changes in stress wave propagation in that direction.

Studies that have used the FFRC method to monitor the decrease in fundamental longitudinal, transverse, and torsional frequencies have shown that for a specific concrete mix, these natural frequencies decrease [15]. However, a trend to quantify this reduction has not been determined. It is the goal of this study to develop a nondestructive, easily employed, impulse device that can be used to determine whether a general trend exists between parameters such as the first longitudinal modal frequency as a function of applied load. This relationship will be investigated as a function of concrete compressive strength. The nondestructive impulse device and measured data will provide engineers a new tool to continue the development of the understanding of long-term, structural health monitoring of concrete subjected to repeated loading.

In order to obtain the necessary data, the variations in longitudinal compression wave velocity and energy absorption of a variety of concrete specimens subjected to fatigue loading conditions were investigated. The details of the newly developed nondestructive device, concrete mixes, instrumentation, experimental setup, and the methods of measurement and analysis are provided. The theoretical background applying to wave propagation in elastic solid media is briefly discussed. The measurement results of the changes in dynamic properties as well as the cumulative energy absorbed during cyclic loading of several concrete mixes are presented and a new relationship to predict damage accumulation is developed and compared with existing relationships. This newly proposed relationship is shown to more accurately predict the behavior between damage and fatigue loading in comparison to previously developed relationships.

## 2. Instrumentation Development

In order to be able to obtain frequency measurements more efficiently during the concrete testing, a new nondestructive excitation device was developed. There were several iterations of the design during the development of the new excitation device. However, throughout all the iterations the core design philosophy remained consistent. When a copper coil is subjected to a voltage, a magnetic field is produced. By placing a series of magnets within this copper coil, the magnets are forced to move directly with the change in voltage. When the magnets reside in a free boundary condition, they move up and down within the coil. However, when one or more of the boundary conditions are fixed, they exert an impulse on that fixed-end surface. By placing a spring loaded series of magnets within a copper coil, the free end of the magnets can be set against a surface in order to exert a short-duration impulse force against it. Thus, it was decided to build a device to produce short duration impulse forces using these concepts. The core design consisted of a spring-loaded series of magnets surrounded by a copper wire coil.

Originally, the coil and magnets were fitted into a PVC housing to provide the coil and springs a fixed position. This housing was intended to sit flush against one end of the concrete cylinder to force the magnets against the concrete surface as it was loaded cyclically. This would ensure that the impulses produced by the movements of the magnets would exert a force onto the cylinder. Because the PVC housing could not support the applied loads to which it was subjected during the tests, a specialized aluminum end plate was fabricated to allow the device to sit on the end of the concrete specimen during compression tests. A similar aluminum end plate was fabricated so that a unidirectional accelerometer could be mounted on the opposite end to measure the wave propagation created by the excitation device. These end plates were designed so that they would work with a typical end capping plate used during standard concrete specimen compression tests. However, there was a hole in the center of each end plate where the device sat during compression tests.

It was quickly discovered that the PVC housing simply was not rigid enough to provide adequate protection for the magnetic coil. The neoprene pads that are typically placed

Figure 1: Final design of the excitation device.

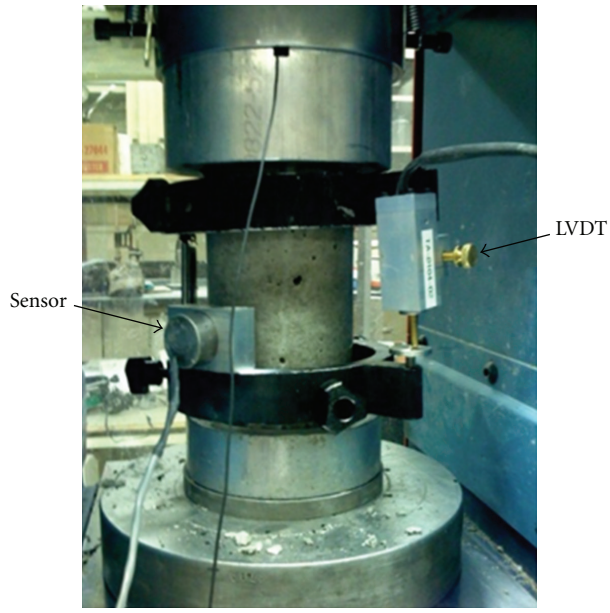


Figure 2: Final configuration for the experiment (LVDT on right, excitation device on left, concrete cylinder fitted with an extensometer yolk, and capped specialized aluminum end plates; the accelerometer was mounted on top of cylinder inside the end plate).

in the end capping plates were continuously compressing the PVC housing during the compression tests causing the entire device to be crushed. Therefore, the design was reduced in size to avoid being crushed by the neoprene pads. The new design consisted of two small steel plates connected to a series of magnets surrounded by a small copper coil. The entire assembly was then protected with a thin plastic tube. The plastic tube restricted the movement of the copper coil; however, and the modified design was disregarded.

The original design was then modified to include a stronger housing. Several copper coils were made and fit into aluminum and steel tube housings. However, the end of the coils was continuously crushed during the compression tests. A coil was then fit into a steel housing and potted with epoxy for protection. This design worked adequately initially, but due to the creep of the epoxy, the coil crushed inwards under load towards the spring-loaded magnet assembly and the magnets were not able to freely move. Finally, an aluminum tube was placed on the interior of a magnetic copper coil that was housed in a steel tube. The entire assembly was potted with 17.2 MPa (2500 psi) epoxy. The steel housing was comprised of a hollowed out 38.1 mm (1.5 in.) circular steel member. The walls of the housing were 5 mm (0.2 in.) thick. The aluminum tube had a 13 mm (0.5 in.) outer diameter and the walls were approximately 1.7 mm (0.1 in.) thick. The epoxy potting extended approximately 8 mm (0.3 in.) from the top of the steel housing making the entire structure approximately 41 mm (1.6 in.). The magnetic core was comprised of three 6 mm $\times$ 5 mm (0.3 in. $\times$ 0.2 in.) neodymium magnets wrapped and fitted in shrink tube. This final design of the excitation device allowed continuous measurements while the specimen was being subjected to cyclic loads. The final design is shown in Figure 1.

Because of the intense pressures associated with the cyclic compression tests, it was discovered that the recorded data also included a great deal of background noise. As a result, it was very difficult to interpret the correct longitudinal frequencies and associated half power bandwidths. An experiment to mount the excitation device on the side of the specimen was conducted, and it was found that adequate energy was produced in the longitudinal direction to allow for this configuration. Another benefit of this side attachment was that the device could be attached to concrete specimens other than cylinders to monitor the structural health. The excitation device was placed into an aluminum housing to increase the long-term durability. Figure 2 shows the excitation device attached to the side of a concrete cylinder along with an extensometer to measure static axial stress-strain behavior during the cyclic tests. This configuration was used throughout all the testing.

## 3. Experiment

A compression machine controlled by a servo unit capable of loading and unloading the concrete specimens at regulated rates was used to apply the predetermined force to the cylinders at specified percentages of their ultimate compression strength. Simultaneously, the linear voltage displacement transducer (LVDT) on the extensometer-measured changes in axial length that was used to calculate strain. From this data, load-deflection hysteretic curves were created so that a comparison between changes in fundamental frequency and energy dissipation could be obtained. Before and after each loading cycle, the excitation device was turned on and readings of the first longitudinal modal frequency and the half power bandwidth were measured. Each concrete cylinder was then immediately reloaded. Cylinders were repeatedly tested in this manner until failure.

In all, five concrete mixes were tested which included the effects of multiple aggregate types, water-to-cement ratios, and different cement types. This variation in concrete mixes

Table 1: Mix designs for 0.5 cubic feet and 28-day compressive strengths.

| Mix | Cement (lbs.) | Fly Ash (lbs.) | Course aggregate (lbs.) | Fine aggregate (lbs.) | Water (lbs.) | $w/c$ ratio | $f_c'$ (psi) |
|---|---|---|---|---|---|---|---|
| Low strength | 9.5 | 0.0 | 0.0 | 70.0 | 4.9 | 0.51 | 1880 |
| Low/medium strength | 12.6 | 0.0 | 38.6 | 34.0 | 5.4 | 0.43 | 3800 |
| Medium strength | 10.3 | 1.9 | 25.1 | 29.7 | 5.0 | 0.48 | 5350 |
| Medium/high strength | 13.2 | 3.3 | 29.4 | 19.0 | 5.2 | 0.39 | 8920 |
| High strength | Proprietary | | | | | | 12560 |

was chosen in order to measure changes in concrete properties representing a wide range of compressive strengths. The concrete designs ranged in mix proportions and had 28-day compressive strengths ranging from 13.0 to 86.6 MPa (1880 to 12560 psi) (Table 1). Concrete specimens were 100 mm × 200 mm and 151 mm × 301 mm (4 in. × 8 in. and 6 in. × 12 in.) cylinders.

Typical stress-strain curves plotted from measurements of the concrete specimens, when loaded in compression, are assumed to be approximately linear up to roughly 40% of the compressive strength. Thus, cylinders were cyclically tested at loads ranging from 50% to 90% of the compressive strength to allow for a broad testing range of the concrete specimens. In order to produce an ideal experiment, several criteria were established. First, the specimens were loaded to a range at which the measured stress-strain curve became nonlinear, ensuring some type of irreversible damage. Secondly, the desired range of cycles was set to be more than 5, but less than 100. This was to ensure an efficient experiment. Finally, the desired failure would occur gradually, rather than during a single cycle. This final criterion was put into place in an effort to quantify the final stages of damage before failure.

After testing several specimens, it was decided that the most effective and efficient experiment would be as follows. Four cylinders from each strength class were loaded cyclically with an initial load at 80% of their respective ultimate compressive strength. The load was increased each cycle in 1% increments up to 90%. Once the 90% mark was reached, the cylinders were loaded cyclically at that magnitude until failure. This experimentation procedure was selected because it allowed for the results of four cylinders from each strength class to be averaged, exceeding the recommended statistical requirement of three cylinders set forth by ASTM C39. Additionally, it was found that loading the cylinders cyclically at magnitudes less than 80% of the ultimate compressive strength did not induce a very large change in the baseline first mode longitudinal frequency. After each cycle, longitudinal frequencies were measured using the newly developed excitation device, acceleration transducer, and digital signal analyzer.

In addition to monitoring the longitudinal frequency, an extensometer with an LVDT was used to measure the axial displacement of the concrete samples as they were cyclically loaded. These load and displacement measurements were subsequently used to produce hysteretic curves that allowed for the calculation of the energy absorbed by the concrete specimen during each cycle.

## 4. Results

Changes in the fundamental frequency were used to quantify damage accumulation, as the concrete specimens were cyclically loaded to failure. The fundamental frequency of each specimen was calculated based on the principle that when an excitation is produced at a point on an elastic medium, waves radiate from the point where the disturbance occurred in all directions. At great distances from this point of disturbance, however, it may be assumed that all particles are moving either parallel to the direction of the wave propagation or perpendicular to that direction. The particles that are moved in a parallel manner are moved by waves of dilation and produce longitudinal waves [17]. The relationship between the rod (parallel) wave velocity and the properties of the concrete can be described using (1);

$$V_{\text{Rod}} = \frac{V_p}{\sqrt{1-\nu/((1+\nu)(1-2\nu))}} = \sqrt{\frac{E_d}{\rho}}, \tag{1}$$

where $V_{\text{Rod}}$ is the rod wave velocity, $V_p$ is the compression wave velocity of the material, $\nu$ is the poison's ratio, $E_d$ is the dynamic Young's modulus of the concrete, and $\rho$ is the mass density of concrete.

Because (1) shows that the rod-wave velocity is dependent on the dynamic modulus of elasticity, $E_d$, it is apparent that as the stiffness of a material deteriorates (microcracks grow), the rod-wave velocity will also decrease. When a disturbance is produced on a known cross-section and length, $l$, the first longitudinal modal frequency (rod-wave velocity) can be described as [18]

$$V_{\text{Rod}} = f_l \lambda, \tag{2}$$

where $f_l$ is the first longitudinal modal frequency, and $\lambda$ is the wavelength, $2l$.

Thus, by measuring the first longitudinal modal frequency of a specimen, the stiffness of that material ($E_d$) can be determined. Also, as the stiffness varies due to an increase in the number and growth of the microcracks, this variation can be quantified by measuring the first longitudinal modal frequency.

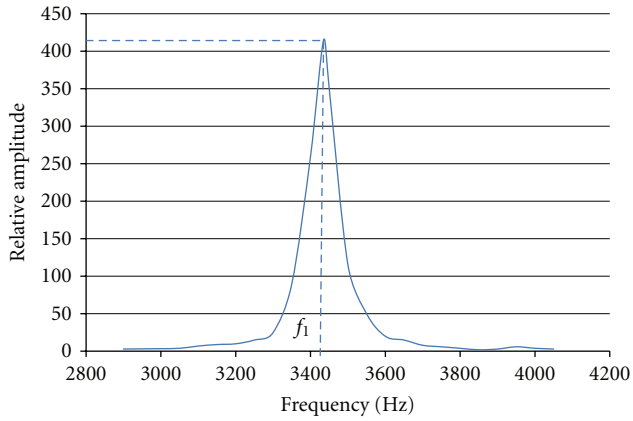


Figure 3: Typical frequency plot and the half power bandwidth.

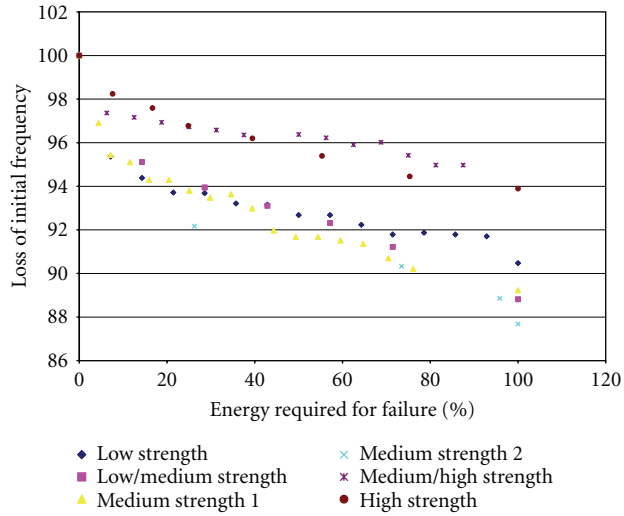


Figure 4: First longitudinal modal frequency as a function of percentage failure.

Measurements of the first longitudinal modal frequencies were recorded at the end of each cycle on every concrete specimen. Simultaneously, load and deflection measurements were recorded using the extensometer and LVDT during each cycle. Initial, undamaged frequencies, $f_o$, were measured before any loading occurred and was used as baseline data. The percent decrease in frequency was determined by dividing each subsequent measured frequency, $f_i$, by this initial frequency. The percentage of failure was taken as the cycle number divided by the total number of cycles required for failure.

A typical frequency versus amplitude plot is presented in Figure 3. As displayed in Figure 3, there was little background noise due to the efficiency of the new nondestructive impulse device. This figure also shows the location of the first longitudinal modal frequency, $f_1$, for use in (2). Based on the output from these plots, the first longitudinal modal frequency could be determined for each concrete specimen. Measured frequencies were plotted against the percentage of failure. Figure 4 presents the general trend of decreasing frequencies as a function of damage (increase in microcracks) for each of the examined concrete mixes. The individual mixes exhibit varying rates of decrease in longitudinal frequency. The values of these variations are listed in Table 2. The data indicates that as concrete compressive strength and therefore tensile strength increase, the percentage loss of first longitudinal modal frequency due to cyclic loading generally decreases. This is presumably due to the increased concrete strength and the inherent reduction in microcracking associated with an increase in tensile strength and stiffness. A discrepancy arises when comparing the low/medium strength and medium strength 1 concrete mixes. Although these two concrete mixes vary in compressive strength by 10.7 MPa (1550 psi), the stronger of the mixes exhibited a higher percentage loss of the first mode longitudinal frequency. After further investigation, it can be noticed that the mixes are very different and that the $w/c$ ratio of the stronger concrete is higher than the weaker concrete. This discrepancy indicates that not only the strength but also the mix ratios could be a factor in the decrease in dynamic properties.

Examination of Figure 4 shows that the longitudinal frequency of any of the concrete mixes decreases as a function of increasing loading. This decrease in fundamental frequency is believed to be a result of microcracks developing in the concrete paste resulting in the degradation of stiffness in the material. As the specimens continued to be cyclically loaded, microcrack growth continued, the concrete became more fatigued, and the longitudinal frequency continued to decrease. Eventually, the coalescence of the microcracks reached a point at which the concrete specimen failed. Figure 4 shows that a trend between the decrease in longitudinal frequency with applied loading and concrete strength is consistent. This conclusion is further supported by the average decrease in longitudinal frequency presented in Table 2. These percent decreases represent the average amount of frequency loss measured on the four cylinders from each concrete mix at the point of failure.

Table 2: Frequency divided by initial frequency.

| Mix | $f_i/f_o$ |
|---|---|
| Low strength | 89.11% |
| Low/medium strength | 90.36% |
| Medium strength 1 | 90.13% |
| Medium/high strength | 92.53% |
| High strength | 93.30% |

The amount of absorbed energy experienced by the concrete during each cycle was calculated from the hysteretic curves measured using the LVDT and extensometer instrumentation. The hysteretic curve represents the amount of axial deflection that is measured for a specific axial load. By measuring the area within the curve, the amount of absorbed energy was quantified for each load cycle. Figure 5 presents the measured energy for each concrete mix as a function of applied load (cumulative damage). The parabolic curve presented indicates that the damage index is nonlinear as predicted by Minor's hypothesis, but of a higher order. The values for the total cumulative energy for each concrete mix

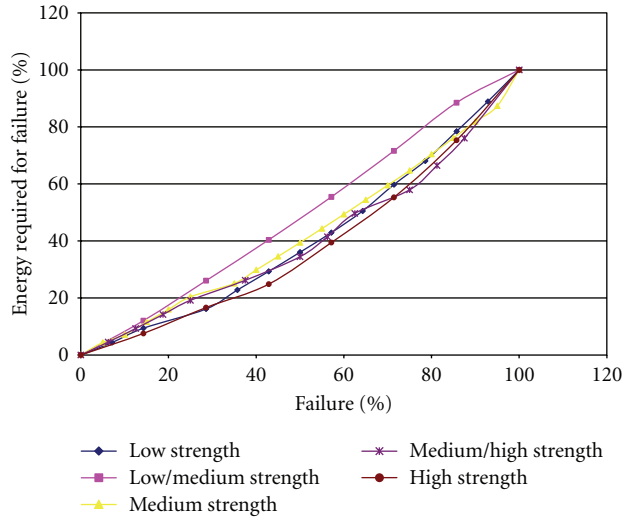


Figure 5: Cumulative energy percentage required as a function of damage.

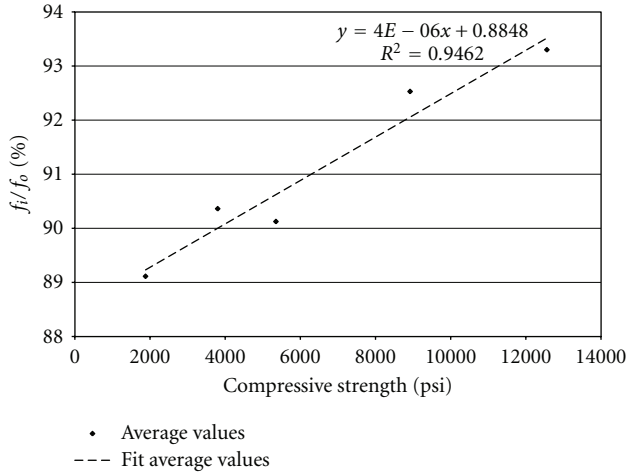


Figure 6: Change in frequency response as a function of compressive strength.

Table 3: Average values of total energy increase per concrete strength.

| Mix | Average total cumulative energy (ft.-lb.) |
|---|---|
| Low strength | 1262 |
| Low/medium | 2318 |
| Medium strength 1 | 2925 |
| Medium/high strength | 2684 |
| High strength | 3528 |

are presented in Table 3. This data indicates that as the concrete strength and associated stiffness increase per mix, the amount of energy ultimately required to cause failure also increases. The compressive strength increase in concrete mixes is typically associated with an increase in strength of the concrete paste. Thus, as the strength of the matrix material increases, the amount of energy required to expand the microcracks that form at the boundary between the matrix material and the aggregate increases. This trend is evident due to the general increase of total cumulative energy required to cause failure presented in Table 3. Again, there is a discrepancy when comparing the low/medium strength and medium strength 1 concrete mixes that is possibly due to specific effects of individual mix ratios.

Thus, as concrete strength increases, the total amount of required energy absorption to cause failure increases. This relationship demonstrates that higher-strength concrete mixes have the ability to absorb more energy during their service life (Table 3). This implies that as the bond between the concrete paste and aggregate increases due to increased concrete strength, more energy is absorbed in modes other than the formation of microcracks.

Figure 6 presents the total average percentage loss of initial frequency as a function of concrete compressive strength. Each data point represents the average of the total loss measured from the four cylinders tested from each compressive strength class at failure. Within each compressive strength class, total frequency loss differed by a maximum of 3.5%. When these values were plotted as a function of compressive strength, a correlation factor of 0.95 was determined. These results indicate that as microcracks develop and grow as loading increases, the first longitudinal modal frequency decreases and is an excellent indicator of damage in concrete specimens as a function of concrete compressive strength.

Figure 7 presents the measured trends of total cumulative energy required to fail a concrete specimen of specific strength. With each ensuing cycle, more damage occurred in the concrete. By measuring the total amount of energy absorbed during all cycles, the total amount of energy that can be absorbed by a specific strength concrete can be determined. Once again, each data point represents the average cumulative energy absorbed from the measurements on the four cylinders from each strength class. The general trend indicates that as compressive strength increases, the total amount of energy required to fail a specimen increases. Within each compressive strength class, cumulative energy absorption differed by a maximum of 11%. When these values are plotted as a function of concrete compressive strength, a correlation factor of 0.75 was obtained.

Finally, the total amount of energy calculated from each measured hysteretic curve is plotted as a function of percentage of failure (Figure 8). The percentage of failure was calculated by dividing the number of current cycles, $N$, by the total number of cycles required to fail the cylinder, $N_f$. This plot presents the determined energy from the extensometer and LVDT from each cycle on all concrete specimens. The trend for the data is exponential, which indicates that it requires less energy (loads) to develop small values of damage (cracks). However, as indicated by the exponential trend of the data, higher amounts of energy are required to induce additional damage. With a correlation of coefficient for all data of 0.95, this plot illustrates that the amount of energy

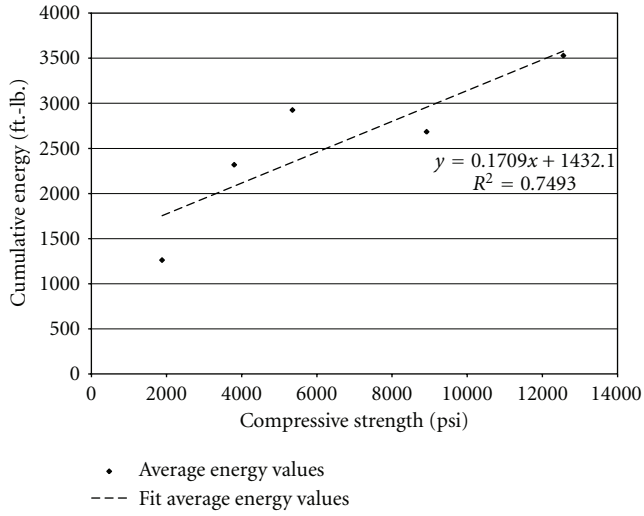


Figure 7: Cumulative energy required for failure as a function of compressive strength.

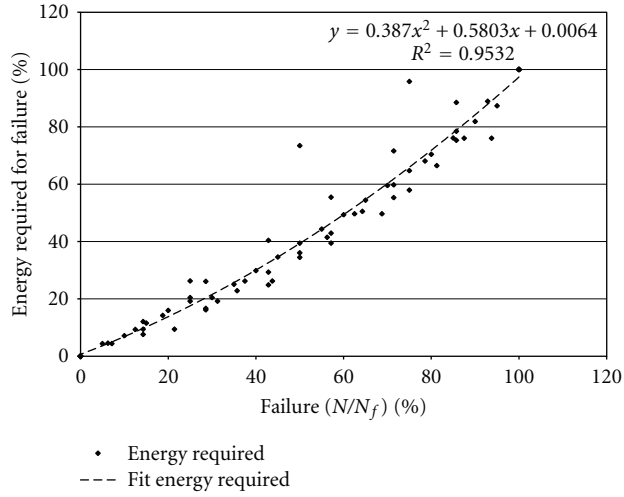


Figure 8: Percentage of total cumulative energy as a function of percentage of failure.

absorbed by a concrete specimen can be used an excellent indicator of damage accumulation.

## 5. Proposed Damage Model

Based on the research results, it was concluded that both changes in fundamental frequency and absorbed energy were excellent indicators of damage accumulation in unreinforced concrete specimens. Thus, both contributing factors were combined to determine a proposed damage model.

Combining the results presented in Figures 6 through 8, an indicator of damage can be developed as functions of compressive strength, energy, and frequency variation for unreinforced concrete. For the explanation provided hereinafter, some rounding occurred while going from scientific notation. From the fitted trend line presented in Figure 8, (3) was developed as

$$\frac{E_i}{E_f} = 0.39D^2 + 0.58D, \tag{3}$$

where $E_i$ is the energy measurement at cycle $i$, $E_f$ is the total cumulative energy required for failure of the specimen, and $D$ is the percentage of damage.

From the fitted trend line in Figure 7, (4) was listed as

$$E_f = 0.17f_c' + 1500, \tag{4}$$

where $f_c'$ is the the compressive strength of the specimen.

Finally, from the trend line presented in Figure 6, (5) was listed as

$$\frac{f_i}{f_o} = 4 \times 10^{-6} f_c' + 0.89, \tag{5}$$

where $f_o$ is the initial frequency, and $f_i$ is the frequency measurement after cycle $i$.

Equation (5) can be solved in terms of $f_c' =$ as (6):

$$f_c' = \frac{(f_i/f_o) - 0.89}{4 \times 10^{-6}}, \tag{6}$$

and by substituting (6) into (4), the following relationship was obtained as (7):

$$E_f = 45900[(f_i/f_o) - 0.89] + 1280. \tag{7}$$

Substituting (7) into (3), an equation to determine the percent damage of a concrete specimen based on the measured first longitudinal modal frequency and hysteretic energy is

$$\frac{E_i}{45900[(f_i/f_0) - 0.89] + 1280} = 0.39D^2 + 0.58D. \tag{8}$$

Finally, solving (8) in terms of damage, the proposed damage relationship is

$$D = \frac{0.0075\left[\sqrt{E_i + 9690((f_i/f_0) - 0.86)} - 99.90\sqrt{(f_i/f_0) - 0.86}\right]}{\sqrt{(f_i/f_0) - 0.86}}. \tag{9}$$

Using the proposed relationship and measured values of energy and frequencies, Figure 9 presents a precise comparison between the newly proposed damage relationship calculated using (9) and the cyclic failure ratio. In Figure 9, the damage index calculated and presented on the $y$-axis presents calculated data based on the data measured at a specific cycle. This damage index is then plotted per cyclic ratio to failure ($N/N_f$ displayed on the $x$-axis). The data in Figure 9 exhibits a parabolic trend indicating that more damage is required during later cycles of loading. This ideology is consistent with the fact that microcracks first form during initial stages of damage, and then grow exponentially towards

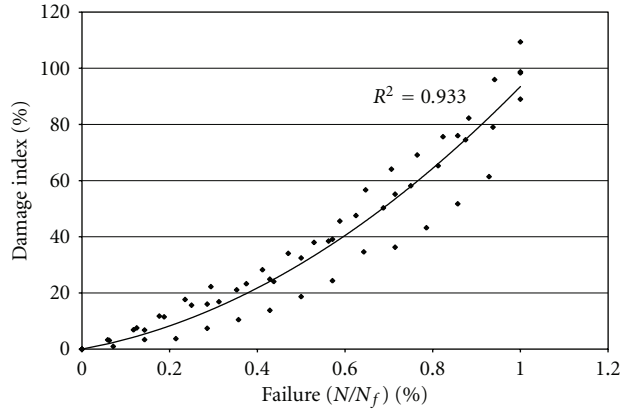


Figure 9: Damage calculated by (9) as a function of the percentage of failure calculated from measured values.

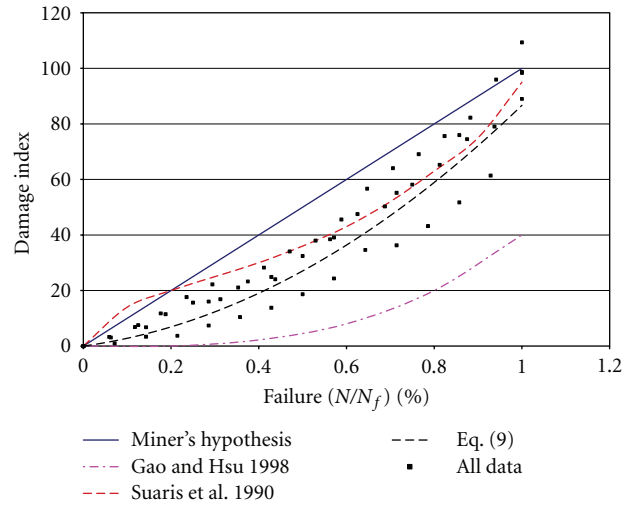


Figure 10: Damage calculated from proposed equation compared with other known damage indices.

failure. Thus, early stages of cyclic loading are associated with lower values of damage and as more loading cycles are applied, an exponential increase in damage is induced upon the specimen. Figure 10 presents a comparison of the damage index calculated using the proposed relationship in addition to several other previously proposed relationships as a function of the percentage of failure. Values calculated with the proposed model correlate to within 6.7% of measured values. Other studies present damage indices that generally increase as a function of percentage of failure. Of these, Miner's hypothesis is the crudest predicting the relationship as purely linear. Gao and Hsu [8] found that the trend was logarithmic but found that at low percentages of failure, the damage index was also relatively low. Finally, Suaris et al. [13] found that there was initial jump in damage at low failure percentage and then a logarithmic increase at mid-to-high levels of failure percentage. The newly proposed relationship (9) demonstrates an exponential trend and differs by a maximum 20%, 54%, and 12%, with Miner's hypothesis, Gao and Hsu [8], and Suaris et al. [13], respectively. Miner's hypothesis values differ from the measured data by a maximum of 24% and an average of 17%. Values using the relationship proposed by Gao and Hsu [8] differ from the measured data by a maximum of 47% and an average of 23%. Finally, values calculated using the equation suggested by Suaris et al. [13] differ from the measured values by a maximum of 13% and an average of 8%. Values calculated using (9) correlate with measured data within 7% indicating that the proposed method is more accurate in predicting the amount of damage induced on cyclically loaded unreinforced concrete specimen in comparison to previous research.

## 6. Conclusions

The long-term, structural health of concrete structures is difficult to quantify. To assist engineers, a new nondestructive, short impulse sensor was developed as part of this research that allowed for automated measurements of unconstrained compression waves through unreinforced concrete specimens subjected to repetitive compressive loading scenarios. This newly developed sensor was used to determine the changes in the first longitudinal modal frequency and damping ratio as a function of cyclic loading to failure. The amount of energy absorbed by individual concrete specimens was calculated based on area of hysteretic curves measured during each cyclic load test. Several concrete mixes were sampled to include a wide range of compressive strengths. The results were used to develop an empirical relationship for damage accumulation. Results indicate the following.

(1) The newly developed short impulse excitation sensor allowed the automated process of accurate measuring unconstrained compression waves through concrete specimens under cyclic compressive loading scenarios to be very efficient and effective.

(2) After a series of cyclically applied compressive loads to failure, the first longitudinal modal frequencies were shown to decrease to a range of 88.5% to 93.3% of their initial, undamaged frequency. In general, higher-strength concretes exhibited less percentage loss of initial frequency at failure.

(3) Using the newly developed sensor, the measurements of total cumulative energy were shown to correlate with percentages of failure to within 4.7%. Also, higher-strength concretes exhibited an ability to absorb more energy at failure presumably due to the stronger concrete paste.

(4) A proposed, empirically derived, damage model was developed as a function of compressive strength, frequency, and energy. This proposed empirical relationship was shown to correlate with measured values to within 7%. Furthermore, the proposed relationship was shown to have a closer correlation than Miner's hypothesis and damage index models proposed from other reviewed research.

(5) The use of this new sensor has potential to be used on any type of concrete structure including, but not

limited to, beams, slabs, and columns. Further testing should be performed to determine its best applications.

## References


[1] A. M. Neville, *Properties of Concrete*, Pearson Education Limited, 4th edition, 1996.

[2] P. S. Rao, B. S. Sarma, N. Lakshmanan, and F. Stangenberg, "Damage model for reinforced concrete elements under cyclic loading," *ACI Materials Journal*, vol. 95, no. 6, pp. 682–690, 1998.

[3] B. Garstka, W. B. Kratzig, and F. Stangenberg, "Damage assessment in cyclically loaded reinforced concrete members," in *Proceedings of the 2nd Cyclically Loaded Reinforced Concrete Members. Structural Dynamics (EURODYN '93)*, pp. 121–128, June 1993.

[4] K. Sadeghi, J. Lamirault, and J. G. Sieffert, "Damage indicator improvement applied on R/C structures subjected to cyclic loading," in *Proceedings of the 2nd Cyclically Loaded Reinforced Concrete Members. Structural Dynamics (EURODYN '93)*, pp. 129–136, June 1993.

[5] Y. J. Park and A. H. S. Ang, "Mechanistic seismic damage model for reinforced concrete," *ASCE Journal of Structural Engineering*, vol. 111, no. 4, pp. 722–739, 1985.

[6] T. T. C. Hsu, "Fatigue of Plain Concrete," *Journal of the American Concrete Institute*, vol. 78, no. 4, pp. 292–305, 1981.

[7] R. Gettu, A. Aguado, and M. O. F. Oliveira, "Damage in high-strength concrete due to monotonic and cyclic compression—a study based on splitting tensile strength," *ACI Materials Journal*, vol. 93, no. 6, pp. 519–523, 1996.

[8] L. Gao and C. T. T. Hsu, "Fatigue of concrete under uniaxial compression cyclic loading," *ACI Materials Journal*, vol. 95, no. 5, pp. 575–581, 1998.

[9] B. Y. Bahn and C. T. T. Hsu, "Stress-strain behavior of concrete under cyclic loading," *ACI Materials Journal*, vol. 95, no. 2, pp. 178–193, 1998.

[10] H. S. Abdelgader and J. Górski, "Stress-strain relations and modulus of elasticity of two-stage concrete," *Journal of Materials in Civil Engineering*, vol. 15, no. 4, pp. 329–334, 2003.

[11] A. Alliche and D. Francois, *Fracture of Concrete and Rock*, Springer, New York, NY, USA, 1989, Edited by S. P. Shah and S. E. Swartz.

[12] W. Suaris and V. Fernando, "Ultrasonic pulse attenuation as a measure of damage growth during cyclic loading of concrete," *ACI Materials Journal*, vol. 84, no. 3, pp. 185–193, 1987.

[13] W. Suaris, C. Ouyang, and V. M. Fernando, "Damage model for cyclic loading of concrete," *Journal of Engineering Mechanics*, vol. 116, no. 5, pp. 1020–1035, 1990.

[14] C. L. Nogueira and K. J. Willam, "Ultrasonic testing of damage in concrete under uniaxial compression," *ACI Materials Journal*, vol. 98, no. 3, pp. 265–275, 2001.

[15] C. Gheorghiu, J. E. Rhazi, and P. Labossière, "Impact resonance method for damage detection in RC beams strengthened with composites," in *Proceedings of the International Society for Optical Engineering*, vol. 5767 of *Proceedings of SPIE*, pp. 205–212, 2005.

[16] P. Shokouhi, "Stress dependency of sonic velocity in concrete under uniaxial load," in *Proceedings of the 87th Annual Meeting of the Transportation Research Record*, 2008.

[17] S. P. . Timoshenko and J. N. Goodier, *Theory of Elasticity*, McGraw-Hill, New york, NY, USA, 3rd edition, 1970.

[18] J. W. S. Rayleigh, *Theory of Sound*, Dover, New york, NY, USA, 1976.